# Mechanical Properties of DU-*x*Mo Alloys with *x* = 7 to 12 Weight Percent

DOUGLAS E. BURKES, RAMPRASHAD PRABHAKARAN, JAN-FONG JUE, and FRANCINE J. RICE

Mechanical properties of six depleted uranium-molybdenum (U-Mo) alloys have been obtained using microhardness, quasistatic tensile tests, and scanning electron microscopy (SEM) failure analysis. U-Mo alloy foils are currently under investigation for potential conversion of high power research reactors to low enriched uranium fuel. Although mechanical properties take on a secondary effect during irradiation, an understanding of the alloy behavior during fabrication and the effects of irradiation on the integrity of the fuel is essential. In general, the microhardness, yield strength, Young's modulus, and ultimate tensile strength improved with increasing Mo content. Microhardness measurements were very sensitive to local composition, while the failure mode was significantly controlled by the impurity concentration of the alloy, especially carbon. Values obtained from literature are also provided with reasonable agreement, even though processing conditions and applications were quite different in some instances.

## I. INTRODUCTION

THE overall goal of the Global Threat Reduction Initiative reactor conversion program has been to develop fuels for nuclear research and test reactors that allow effective conversion from highly-enriched uranium (HEU) to low-enriched uranium (LEU), thereby reducing the threat of nuclear proliferation worldwide.[1] Highly-enriched uranium is defined as a fuel containing greater than 20 pct by weight of the fissile uranium isotope [235]U. Conversely, LEU is defined as a fuel containing less than or equal to 20 pct by weight of the fissile uranium isotope [235]U. A majority of the remaining high power nuclear research and test reactors still operating on HEU fuel have fissile atom density requirements that are too high for conversion to existing LEU fuel elements, *i.e.*, dispersion fuels,[2] since a decrease in uranium enrichment requires an increase in the uranium density to maintain the net fissile atom density of the fuel. This has led to a new pursuit of developing high uranium density monolithic fuel that possesses the greatest possible uranium density in the fuel region. In order to effectively lead this pursuit, new developments in processing and fabrication of the fuel elements have been initiated, along with a better understanding of material behavior as a result of these new developments.

Based on this brief background, metallic uranium alloys are typically better candidates as fuel materials.[3–5] Uranium has some material drawbacks, such as poor oxidation and corrosion resistance, low hardness and yield strength, and lack of dimensional stability of the room temperature α phase. Dimensional stability of the fuel during reactor operation is one of the most important, yet technically challenging, material issues to address. Therefore, the high-temperature γ phase is desired based on isotropy that can be retained at room temperature and better resistance to thermal recycling and radiation damage.[6] In order to stabilize the high temperature γ phase, an alloying element is added, such as molybdenum that has a high solid solubility in bcc γ-uranium.[2] Alloys containing from 5.4 to 20 wt pct Mo (the solid solubility limit of Mo in γ-U) retain the γ phase at room temperature.[7] Swelling resistance, mechanical properties, and oxidation resistance of uranium is improved by increased Mo alloying additions. Alloying above 8 wt pct Mo has little effect on fuels for low burn-up* applications, while alloying above 8 wt pct

---

*Burn-up is defined as the amount of heavy metal, *i.e.*, uranium, in the fuel that has been fissioned. Burn-up can be expressed as either a percent of heavy metal atoms that have fissioned (atomic percent) or in units of fission energy produced per unit mass of heavy metal (GWd/MTHM or MWd/kgHM).

---

Mo shows significant improvements in swelling resistance for higher burn-up applications.[8] Alloys containing less than 4.7 wt pct Mo result in a series of metastable α phases. Thus, uranium-molybdenum (U-Mo) monoliths containing 7 wt pct or greater Mo are the current fuel alloys of choice for conversion of high power research reactors. However, U-Mo alloys are prone to stress corrosion cracking in various environments, requiring an

DOUGLAS E. BURKES, JAN-FONG JUE, and FRANCINE J. RICE, Technical Staff Members, are with the Idaho National Laboratory, Idaho Falls, ID 83415-6188. Contact e-mail: douglas.burkes@inl.gov RAMPRASHAD PRABHAKARAN, Graduate Student, is with the Materials Science and Engineering Department, University of Idaho, Moscow, ID 83844-3024.

appropriate understanding of mechanical properties prior to applying their use on a commercial engineering scale.

Mechanical properties of the fuel have a secondary impact on fuel behavior in terms of irradiation behavior. However, mechanical properties of the fuel are extremely important for overall plate properties. For dispersion fuel types, the matrix containing the fuel particles dominates the overall plate mechanical behavior. For plates containing a monolithic alloy creating a lamellar composite structure, the properties of the foil dominate the overall plate mechanical behavior and failure mode. Understanding this behavior is extremely important for postprocessing operations, such as forming the plates into arced shapes, and potential failure modes during irradiation.

Limited data exist on the property-processing-structure relationship of metallic uranium monolithic fuel foils. Most of the available literature involving properties, specifically for U-Mo alloys, were produced in the 1950s and 1960s for application in fast reactors, where operating temperatures are hundreds of degrees higher than those experienced in a research reactor. For example, this type of alloy was chosen as the initial fuel for the pulsed fast reactor SORA in Italy,[9] the Dounreay Fast Reactor in the United Kingdom, the Enrico Fermi Fast Reactor in the United States, and several fast burst reactors, including Oak Ridge Health Physics Research Reactor (HPRR), Lawrence Livermore Super Kukla, and Sandia APRFR. In these cases, the nuclear fuel was fabricated by extruding the fuel alloy so that mechanical properties and the microstructure obtained was different than fuel being investigated today where cast samples are rolled into relatively thin, monolithic fuel foils. In addition, alloys ranging from 7 to 12 wt pct Mo, fuels of interest, are investigated for completeness and to aid fuel irradiation behavior and performance thermomechanical models.

## II. EXPERIMENTAL DETAILS

Six monolithic foil alloy compositions of depleted uranium ($^{238}$U, <0.3 pct $^{235}$U) and molybdenum were investigated. The alloys are referred to in this article as DU-7Mo, DU-8Mo, DU-9Mo, DU-10Mo, DU-11Mo, and DU-12Mo (nominal weight percentages). Mechanical properties of the monoliths were obtained from tensile tests and microhardness, in addition to microscopy of failed specimens. Physical metallurgy, phase, and impurity analysis of the alloy compositions were also investigated and discussed where appropriate.

### A. Alloy Preparation

Depleted uranium metal feedstock (<0.21 wt pct $^{235}$U, 99.8 pct purity) and molybdenum foil (Alfa Aesar, 99.95 pct purity) were alloyed with a Centorr Model 5SA single arc furnace (Centorr Vacuum Industries, Nashua, NH). Alloyed ingots were melted three times to achieve adequate homogenization, flipping the button

for each melt. Ingots were melted and cast into a graphite book mold, yielding coupons approximately 38-mm long × 25-mm wide × 3-mm thick, each weighing 30 to 35 g. Coupons were dressed and trimmed to fit into three-layer 1018 carbon steel frame assemblies, followed by welding of the assembly edges to create a hermetically sealed "can." All melting, casting, and welding operations were performed in an argon glovebox (purity of <5 ppm $O_2$; <10 ppm $H_2O$). Cans were preheated in a box furnace at 650 °C for 45 to 60 minutes prior to hot rolling to create the monolithic foils. Cans were passed through a Fenn two high rolling mill several times, with an initial reduction of 10 pct and decreased to 3 pct as processing continued. After five passes the cans were placed back into the box furnace in order to reheat the assembly to 650 °C. Rolling was repeated until the desired foil thickness of approximately 254 $\mu$m was obtained. Once the desired foil thickness was achieved, foils were placed back into the box furnace for a final annealing step at 650 °C for 120 minutes. Additional information on processing of the monolithic foils can be found in Reference 10.

### B. Specimen Preparation

The monolithic alloys were removed from the carbon steel can by shearing the edges. A metallographic specimen was cut from the foils and cold mounted in the longitudinal direction. A phase analysis sample and chemical analysis sample was also taken from the foils. The remainder of the foil was used to prepare the tensile test specimens by placing a section of the foil in a hardened carbon steel punch and die set and producing a "dogbone" specimen. The overall dimensions of the tensile test specimens were 3.81-cm long by 0.953-cm wide, with the gage section being 1.43-cm long and 0.478-cm wide. All specimens were subjected to a chemical "cleaning" in 30 pct nitric acid for 10 to 30 seconds followed by rinsing with de-ionized water. In the case that analysis was not conducted concurrent with the cleaning process; specimens were vacuum sealed in polyurethane bags to prevent oxidation.

### C. Metallography, Microhardness, and Failure Analysis

Cold mounts containing foils in the longitudinal (rolling) direction were ground and polished to a 6-$\mu$m surface finish for each alloy. Mounts were etched in solution of 70 pct phosphoric acid, 25 pct sulfuric acid, and 5 pct nitric acid with times ranging from 45 to 150 seconds depending on alloy composition for optical microscopy. Vickers microhardness measurements were carried out using a LECO LM 100 microhardness tester (Leco Corporation, St. Joseph, MI) in each direction across the foil cross section at room temperature with a 100 $g_f$ load and a 15 second dwell time, following ASTM Standard E384-06. Data presented are average and standard deviations of at least eight indentations. Scanning electron microscopy (SEM) of one fractured surface for each alloy was conducted using a Zeiss DSM960A digital SEM (Carl Zeiss SMT Inc., Peabody, MA) to determine the mode of failure.

## D. Phase and Impurity Analysis

The X-ray diffraction (XRD) analysis was conducted by placing a square flat section of the foil, approximately 0.5 inch on edge, in a zero-background slide and covered with Mylar$^{\copyright}$ film to avoid spread of contamination. Analysis was conducted by scanning from 30 to 120 $2\theta$ deg at a scan rate of 1.0 deg·s$^{-1}$ using a Scintag X1 powder diffractometer (ThermoARL, Franklin, MA) in theta-theta geometry. The X-ray tube operated at a voltage of 45 kV and a current of 40 mA. Impurity analysis was conducted to determine the amount of carbon impurity in the alloys using a LECO IR-412 carbon determinator (Leco Corporation, St. Joseph, MI) with an HF-400 induction furnace.[11]

## E. Tensile Tests

An Instron 3366 universal testing machine (Instron Corporation, Norwood, MA) with adequate ventilation was employed to conduct tensile tests at room temperature with a strain rate of $5.83 \times 10^{-4}$ s$^{-1}$. A total of at least five specimens were analyzed for each alloy. Data were logged to a desktop computer at a frequency of 10 Hz. Engineering stress ($\sigma$)–engineering strain ($\varepsilon$) diagrams were constructed from load ($P$)–displacement ($\delta$) data. Ultimate tensile strength ($\sigma_u$) was calculated from the $\sigma$-$\varepsilon$ data, while a chord method was employed to determine the Young's modulus ($E_t$) from the linear portion of the $\sigma$-$\varepsilon$ diagrams. Yield strength ($\sigma_y$) was determined using a 0.2 pct offset. Percent elongation of the samples ($e_f$) was determined from displacement data at failure and the initial sample length.

## III. RESULTS AND DISCUSSION

### A. Metallography and Microhardness

Optical metallographs of the six alloys investigated taken in the longitudinal direction, i.e., parallel with the rolling direction, are provided in Figure 1. Observation of the optical metallographs reveals differences in the amount of banding present across the grains that mainly occurs in the central areas of the foil. In each alloy, recovery and recrystallization of the microstructure appears to have occurred upon final rolling and annealing treatment at 650 °C for 2 hours. The grains appear to be coarser and much more equiaxed in nature for lower Mo contents, with the amount of grain anisotropy increasing with increased Mo contents along with the generation of finer grains. Grain sizes range from approximately 21 $\mu$m in diameter for the DU-7Mo to 10 $\mu$m in diameter for the DU-12Mo.

There appears to be no direct dependence on the amount of banding on Mo content. The DU-9Mo, DU-10Mo, and DU-12Mo alloys all show a significant amount of banding, while the DU-8Mo alloy shows minimal banding. The banding effects are relatively random and result from inadequate homogenization of the Mo into the U due to the significant differences in melt temperature. The inadequate homogenization results in Mo-rich and Mo-lean zones that retain the quenched $\gamma$-phase structure. The banding is not the result of decomposition in $\alpha'$ or ordering into $\gamma^0$ during casting, rolling, or annealing, as these would result in not only different types of bands, but would also be evident from the metallography and additional phase analysis, given the large degree of banding in some of the alloys. Electron microprobe analysis has been conducted on U-Mo alloys containing 8, 10, and 12 wt pct Mo that showed large variations in Mo content from the center of the grain to the grain boundaries.[12] The range in variation increased significantly with increasing Mo contents. Similar banding has also been observed for U-Nb with the Nb content ranging from 4.7 to 7 wt pct across the grains.[13] Electron microprobe analysis (EPMA) was not conducted on the alloys in this study.

Vickers hardness values as a function of molybdenum content are provided in Figure 2. Observation of this figure clearly shows an increase in the Vickers hardness number as the molybdenum content increases. The increase in the hardness of the DU-Mo alloys is believed to result from solid solution hardening of the $\gamma$ phase with increased Mo content.[5,14,15] The Vickers hardness increases linearly with exceptional correlation from Mo contents ranging from 8 to 11 wt pct Mo. However, both the DU-7Mo alloy and the DU-12Mo alloy are slightly above the linear trend.

Using the equation generated from data in the range of 8 to 11 wt pct Mo, the hardness obtained for the nominal 12 wt pct Mo alloy is much closer to 14 wt pct Mo, and that for the nominal 7 wt pct Mo alloy is close to the 8 wt pct Mo alloy. Based on EPMA results conducted by Nomine et al. on a U-12Mo alloy, the Mo variations could be as high as 15 wt pct Mo at the grain center that result in a Mo lean zone at the grain boundary (thus maintaining the nominal Mo concentration).[12] Observation of the metallographs in Figure 1 revealed a significant amount of chemical banding in the DU-12Mo that resulted from inadequate homogenization during the melt and cast operation. The darker bands in the metallographs are Mo rich, have a high aspect ratio, and are more closely spaced than the other alloys containing significant banding (DU-7Mo, DU-9Mo, and DU-10Mo). The grain size for the DU-12Mo alloy was 9.1 $\mu$m, and an average diagonal of 23.1 $\mu$m was obtained for the hardness testing. Thus, the diagonal will include a significant portion of the chemical banding, or Mo rich zones, resulting in the higher hardness value for this alloy. The chemical bands for the DU-7Mo, DU-9Mo, and DU-10Mo alloys have similar aspect ratios, but are more widely spaced than the bands for the DU-12Mo alloy. Furthermore, the grain size increases with decreased Mo contents, as does the average diagonal of the hardness measurement. The hardness of the DU-7Mo and DU-12Mo alloys should follow the predicted trend as determined for $x = 8$ to 11 by increasing the load employed to obtain the measurements; thus taking into account an increased number of grains and average, rather than just a local measurement. Values from literature are close to the experimental values for this study and the predicted trend.
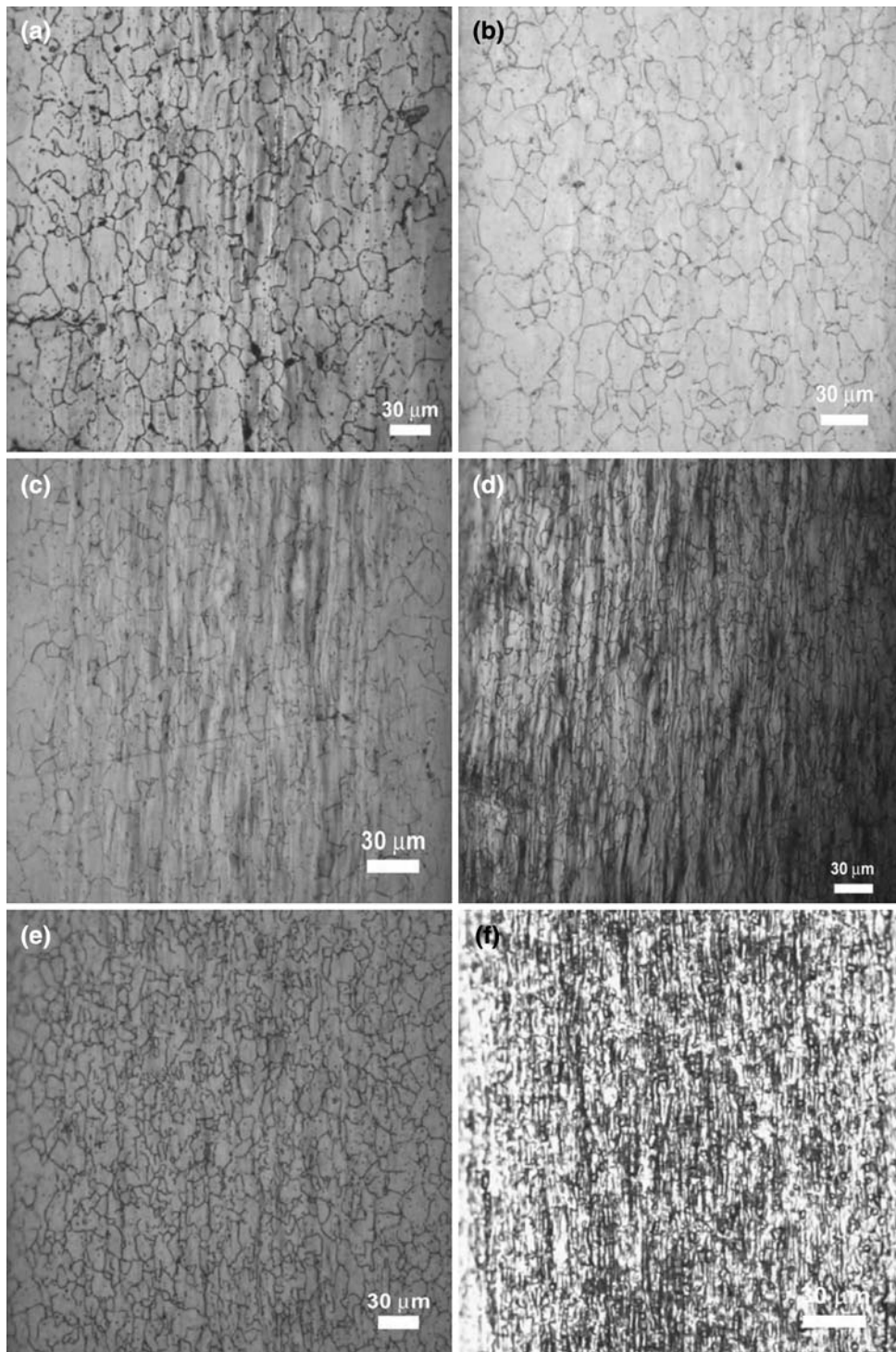
Fig. 1—Optical metallographs as a function of Mo content taken parallel with the rolling direction for (*a*) DU-7Mo, (*b*) DU-8Mo, (*c*) DU-9Mo, (*d*) DU-10Mo, (*e*) DU-11Mo, and (*f*) DU-12Mo. Degree of deformation banding and grain size fluctuates as a function of Mo content.

The slight differences can be attributed to the different loads used during measurement, *i.e.*, measurements in the current study were using micro-indentation loads ($\leq 200$ $g_f$) while those in previous literature were using indentation loads when reported (~$kg_f$). This observation shows the sensitivity of the hardness measurement to both local composition and indentor load and must

be considered when making a direct comparison of measurements.

It is important to note that while the increase in microhardness is believed to result from solid-solution strengthening of Mo, Hall–Petch strengthening might also influence the measurements since grain size decreases with increasing amounts of Mo. Previous
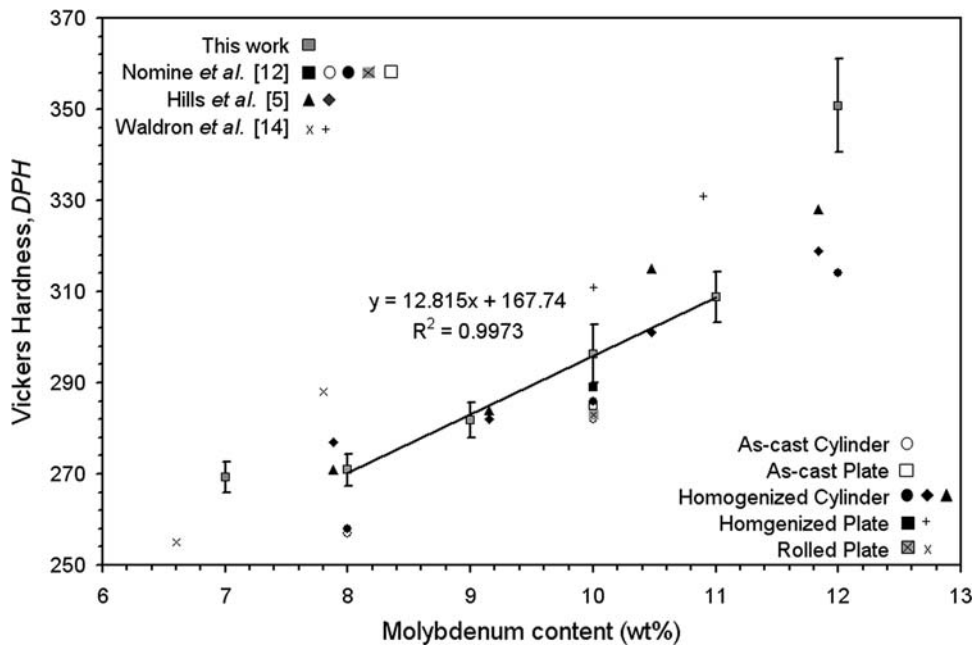
Fig. 2—Average Vickers microhardness values of fuel foils as a function of Mo alloying content. Hardness values are observed to increase with increasing Mo content.

literature does not provide grain size as a function of Mo content enabling deconvolution of the effects challenging at this time. Obviously, further experimentation is necessary to understand these effects better.

### B. *Phase and Impurity Analysis*

X-ray diffraction patterns of the six alloys investigated are provided in Figure 3. Each of the major peaks is indexed to $\gamma$-U, as expected. The maximum peak location varies for each of the alloys; owing to the classical bcc textured nature of the microstructure imparted by the hot-rolling process, and appears to be independent of Mo content. There is no significant evidence of $\gamma$-phase decomposition observed in the XRD patterns, either to $\alpha$ phase or ordering to the $\gamma^0$ phase. Ordering to the $\gamma^0$ phase will consist of only a slight variation in the crystal structure,[16,17] and was not observed in XRD patterns evidenced by the lack of splitting of the major $\gamma$-U peaks into two peaks (representing $\gamma^0$ phase).

Carbon analysis performed on each of the DU-Mo alloys did not show a clear dependence of impurities upon molybdenum content. Alloys ranging from 8 to 11 wt pct Mo had carbon concentrations less than 65 ppm, while the DU-7Mo had a carbon concentration of 100 ppm and the DU-12Mo alloy a carbon concentration of 290 ppm. Carbon impurities have very low solubility in uranium. For example, U-Mo alloys typically contain only primary UC carbides with polyhedral shapes distributed randomly within the grains and at the grain boundaries.[12] Carbon has little effect on the alloying behavior between uranium and molybdenum, other than introducing inclusions of uranium carbide in the matrix that is typically enriched with molybdenum in proportion to the amount of uranium carbide preferentially formed.[18] However, inadequate
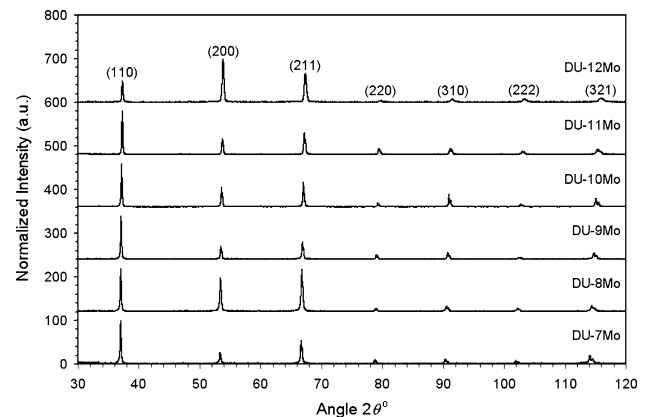


Fig. 3—XRD patterns of the six monolithic DU-Mo alloys investigated. Each diffraction pattern reveals the presence of the expected $\gamma$-U phase.

homogenization of a cast alloy or absence of a homogenizing treatment can result in an uneven distribution of carbon and an irregular grain size. Thus, UC inclusions can adversely affect the desired properties of the alloy in terms of grain growth, deformation mechanism, and transformation kinetics. Carbon concentration is introduced from the graphite molds used for the casting operation. As there are no intentional differences in the casting process, the variation in carbon concentration is most likely the result of inadequate cleaning of the mold prior to casting or deviations in casting temperature as carbon reacts rapidly with uranium in a molten state. Evidence of the impact of carbon on grain growth can be observed in the DU-12Mo alloy, which had a different microstructure in terms of grain size uniformity and recrystallization than the other five alloys investigated.

## C. Tensile Tests

Some sample engineering stress-strain curves for a DU-8Mo and DU-10Mo alloy foil are provided in Figure 4. None of the alloys investigated reveal cracking prior to yield and fracture, *i.e.*, this not a significant departure from the expected elastic behavior of the alloys. Note the gain in ductility (elongation) with increased Mo content. Results of the tensile tests are summarized in Figures 5 through 8 for 0.2 pct offset yield strength, Young's modulus, ultimate tensile strength, and percent of elongation. Also included on each of the curves are comparative values from literature.

The 0.2 pct offset yield strength, modulus of elasticity, and ultimate tensile strength all improved linearly with good correlation with increasing molybdenum content.
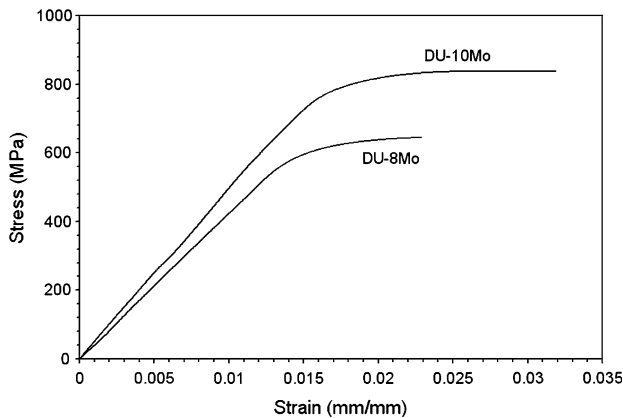


Fig. 4—Sample engineering stress-strain diagrams for a DU-8Mo (52 ppm C) and DU-10Mo (54 ppm C) alloy foils. Increase in mechanical properties with increasing Mo content is observed from the sample diagrams.

The gain in these properties is attributed to the improved resistance to bulk plastic deformation through the increased addition of Mo and associated hardening effect in the $\gamma$ phase. Modulus of elasticity and 0.2 pct offset yield strength values obtained from the current study follow similar trends to values available in literature. However, in each case, the values from the current study are typically lower than those available from literature. With the exception of values published by Waldron *et al.*,[14] the same is true for the ultimate tensile strength observations.

There are many significant differences between studies conducted by previous researchers and that of the current authors making direct comparison of the results challenging. Examples of these differences include fabrication history, homogenization, and postprocess treatments, strain rates, carbon impurity content, and specimen geometry. These differences are summarized in Table I for each set of data used as a comparison.

There are two major differences between the conditions defined for the current work and those of previous researchers: homogenization treatment and sample geometry. It is also possible that the differences in strain rate could impact the variation in mechanical property values since bcc metals tend to be strain sensitive. However, since the strain rates listed in Table I are comparable, this effect is believed to be secondary to homogenization treatment and sample geometry, although further experimentation is necessary.

First, the chemical banding observed in the metallographs and discussed to cause the hardness discrepancies resulted from inadequate homogenization upon casting the alloys for the current work. No homogenization treatment was performed after casting, as done for all of the comparative literature. Considering Nomine *et al.*
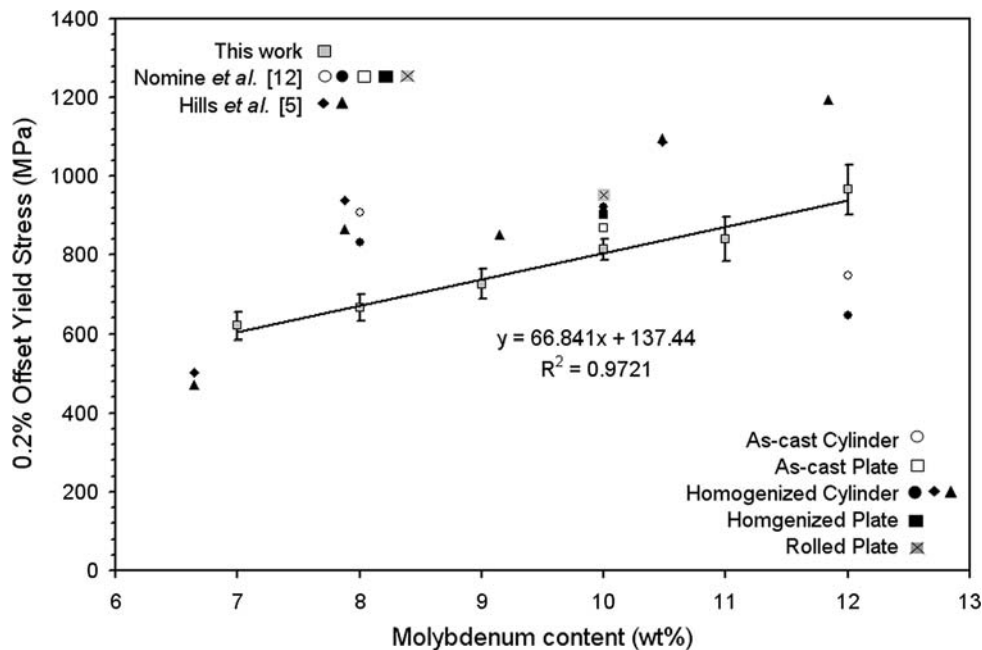


Fig. 5—Average 0.2 pct offset yield strength of the alloys as a function of Mo content. The 0.2 pct offset yield strength increases linearly with increasing Mo content.
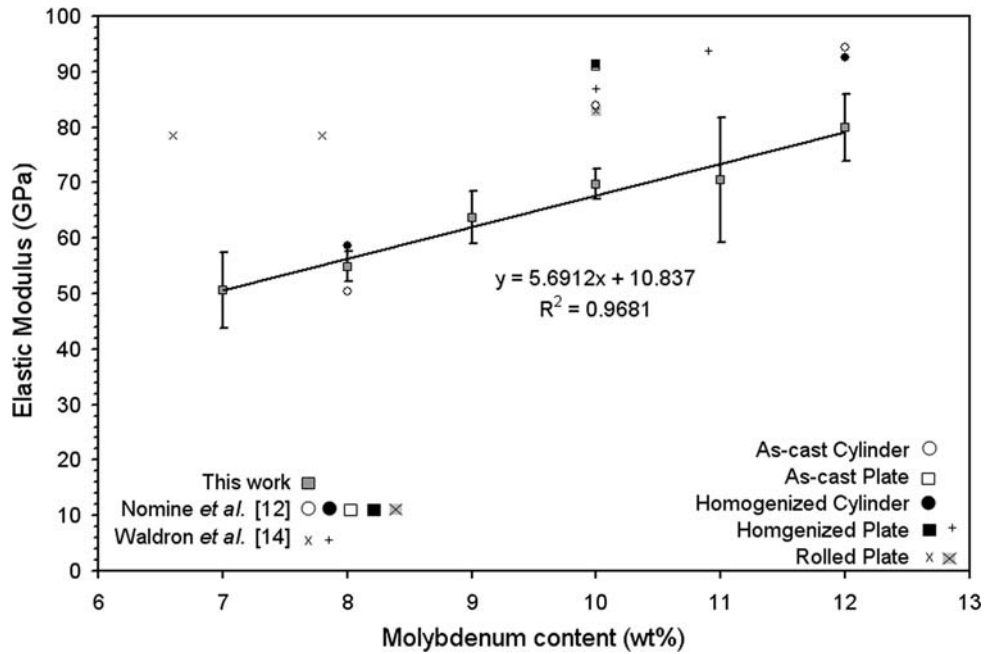
Fig. 6—Average elastic modulus of the alloys as a function of Mo content. Elastic modulus increases linearly with increasing of Mo content.
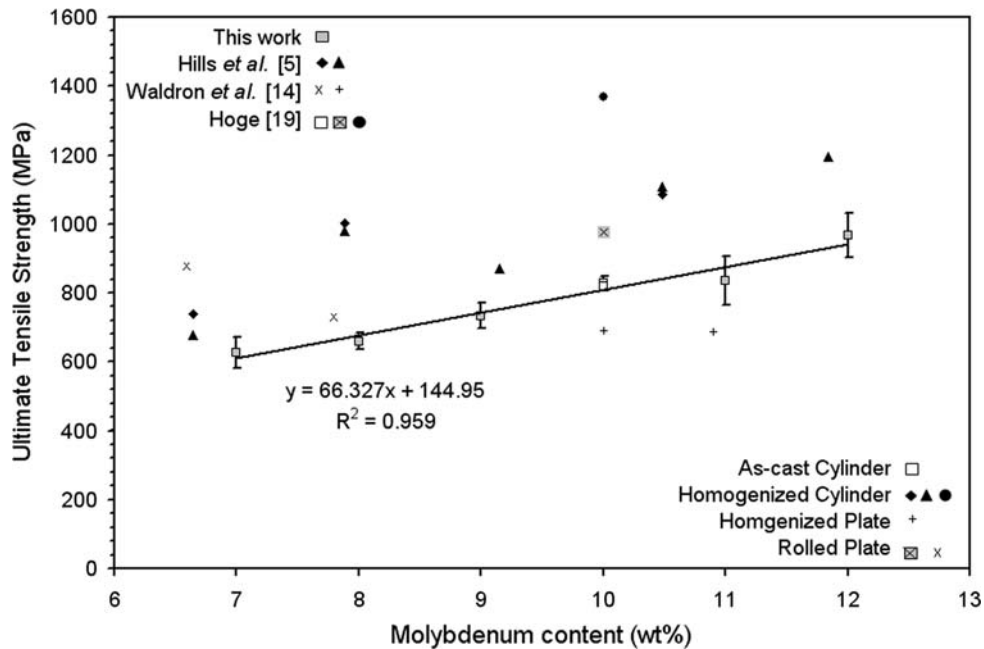


Fig. 7—Average ultimate tensile strength of the alloys as a function of Mo content. Ultimate tensile strength increases linearly with increasing Mo content.

results on the U-10Mo alloy, an increase in yield strength is observed between an as-cast plate and a homogenized plate.[12] The as-cast plate yield strength, undergoing no homogenization treatment, is much more comparable to the current data than samples that were subjected to a homogenization treatment. The same trend for the remaining alloys compared holds true with the exception of Hills et al. U-6.6Mo alloy[5] and Nomine et al. U-12Mo alloy. A similar observation

can be made concerning ultimate tensile strength between the current work and that of Hoge.[19] As provided in Table I, Hoge investigated three different states on a U-10Mo alloy. The alloy tested in an as-cast state with no homogenization has almost the same UTS value as that obtained in the current study, even through the carbon concentration was four times higher in Hoge's alloy. The UTS increased significantly with homogenization treatment after casting. The trend holds

true for alloys investigated by Hills *et al.*,[5] but not necessarily for those of Waldron *et al.*[14]

The second difference is most likely an artifact of the sample geometry and the experimental configuration of the particular author. For the current investigation, relatively thin foils were used to obtain the mechanical properties, given the particular application. The sample thickness to grain diameter ratio for the alloys ranged from 17 to 32. The test specimens used in Hills *et al.* and Nomine *et al.* studies had a diameter of 3 mm, while
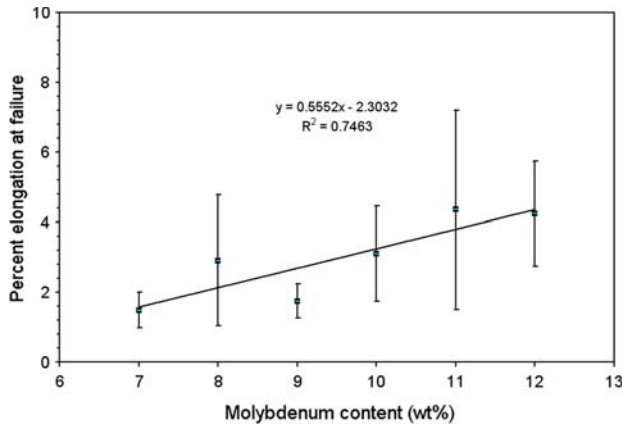


Fig. 8—Average percent of elongation of the alloys as a function of Mo content. Percent of elongation increases near linearly with increasing Mo content, but shows high variability evidenced by the large error bars.

that of Hoge was 9 mm.[5,12,19] Although the specific grain sizes were not explicitly reported in these studies, comparable results on metallographic studies place grain diameters ranging from 0.1 to 3 mm in diameter, physically plausible given larger casting batches and the extended homogenization conditions after casting. Typically, a cylindrical specimen containing isoaxed grains should have a diameter equal to at least 30 to 40 times that of the grain diameter.[20] If this were indeed the case, the typical thickness-to-grain diameter ratio would have been violated for previous results (as is typical for coarse-grained materials), and thus a direct comparison between values is extremely challenging. The yield and flow stress of the alloys would have been undoubtedly altered by such a violation. This is converse to the prediction of the typical Hall–Petch relation. However, since the grain size range between current and previous studies are orders of magnitude different, the Hall–Petch approximation must only be valid over a narrow range for the U-Mo alloys. This could be the reason why the information obtained from the current study is much more consistent than that compared to previous researchers, although without specific grain diameters of specimens tested previously some speculation still remains. The tensile specimens in the current work were very notch sensitive, an observation also noted by Hoge with hot-rolled material, but not by Nomine *et al.* The notch sensitivity, particularly with the thinner specimens, could also play a role in the lower yield and ultimate tensile strengths observed.

Table I. Summary of Alloys, Fabrication History, Strain Rate, Impurity, and Geometry Used by Previous Researchers Compared to the Current Work

| Alloy | State | Strain Rate ($\times 10^{-3}$) s$^{-1}$ | Carbon Impurity (ppm) | Specimen Geometry | Author |
|---|---|---|---|---|---|
| U-8Mo, U-10Mo, and U-12Mo | as-cast | 0.833 | 100 | cylindrical | Nomine[12] |
| U-8Mo, U-10Mo, and U-12Mo | homogenized for 24 h at 1000 °C with compressed air quench | 0.833 | 100 | cylindrical | Nomine[12] |
| U-10Mo | homogenized (as above), rolled with 56 pct reduction at 900 °C and annealed at 600 °C for 1.5 h | 0.833 | 100 | plate/rolled plate | Nomine[12] |
| U-6.6Mo, U-7.9Mo, U-9.2Mo, U-10.5Mo, and U-11.8Mo | homogenized at 950 °C for 72 h with air quench followed by annealing at 950 °C for 0.5 h and mercury quenched | 1.00 | 410 | cylindrical | Hills[5] |
| U-6.6Mo, U-7.9Mo, U-9.2Mo, U-10.5Mo, and U-11.8Mo | homogenized at 950 °C for 72 h with air quench followed by annealing at 950 °C for 0.5 h and oil quenched | 1.00 | 410 | cylindrical | Hills[5] |
| U-10Mo | as-cast | 0.048 | 800 | cylindrical | Hoge[19] |
| U-10Mo | homogenized for 24 h at 900 °C | 0.048 | 71 | cylindrical | Hoge[19] |
| U-10Mo | homogenized (as above), rolled with 19 passes at 982 °C and annealed at 750 °C for 18 h | 0.048 | 98 | cylindrical | Hoge[19] |
| U-6.6Mo and U-7.8Mo | homogenized at 900 °C for 168 h | NL* | 700 | rolled plate | Waldron[14] |
| U-10Mo and U-10.9Mo | homogenized at 900 °C for 168 h | NL | 700 | plate | Waldron[14] |
| DU-7Mo, DU-8Mo, DU-9Mo, DU-10Mo, DU-11Mo, and DU-12Mo | rolled with 90 pct reduction at 650 °C and annealed at 675 °C for 2 h | 0.583 | 20 to 290 | rolled foil | this work |

*NL: not listed.

The percent of elongation does not reveal any clear trends with respect to molybdenum content. In fact, the percent of elongation varies randomly based on where the sample was taken from within the rolled foil, owing both to the notch sensitivity of the rolled alloys and to the variations in carbon impurity. This is evidenced by the significantly large standard deviation values. In general, the DU-Mo alloys are not very ductile in nature. Ductility could be lessened by nonmetallic inclusions[14] or by precipitates that form from impurities in the alloy, ultimately having an embrittling effect on the mechanical behavior. Casting processes must not be overlooked as a contributing factor in the mechanical behavior discrepancies. Some data exists that suggests alloys prepared with advanced casting techniques are more ductile.[21] The low extension suggests that it is easier for the sample to continue deforming in a localized area once deformation has been initiated rather than initiating more deformation in another location.[5]

### D. *Failure Analysis*

The SEM photomicrographs of a sample fracture surface for each of the DU-Mo alloys investigated are provided in Figure 9. The DU-12Mo alloy was observed to fail by a dimple rupture failure mode. The DU-12 alloy contained 290 ppm C, the highest impurity concentration of all the alloys investigated. The carbon introduces inclusions of uranium carbide in the matrix typically enriched with molybdenum in proportion to the amount of uranium carbide preferentially formed.[18] These second-phase inclusions create regions of localized strain discontinuity that nucleate microvoids. The microvoids began to grow and coalesce as the deformation of the foil continued, eventually creating a continuous fracture surface and the cuplike dimples observed in Figure 9(f). The fact that the dimples observed in the fractograph are small and numerous in number suggests that there were many closely spaced second-phase inclusions in the microstructure causing the microvoids to coalesce before they had an opportunity to coarsen, similar to observations made in oxide dispersion strengthened materials.[22] Thus, failure of the DU-12Mo alloy occurred *via* a full-slant fracture by combined modes I and III, *i.e.*, tearing and shearing, represented by the lack of macroscopic fracture direction indicators but the presence of a few elongated dimples and many essentially equiaxed dimples with a full shear lip.[23]

The DU-8Mo, DU-9Mo, DU-10Mo, and DU-11Mo alloys (Figures 9(b) through (e)) all failed by decohesive rupture along the equiaxed grain boundaries. The fractures are all predominately intergranular. These alloys contained the lowest impurity concentrations of all six alloys investigated with carbon concentrations less than or equal to 65 ppm. Typically decohesive rupture results from hydrogen embrittlement or stress-corrosion cracking (SCC). The SCC occurs in an essentially transgranular (through the grains) fashion and follows the low and high Mo zones indiscriminatingly.[16] Samples containing between 8 and 11 wt pct Mo were all observed to fail intergranularly (along the grain boundaries), suggesting that SCC did not play a

significant role in failure. The tensile test strain rate is important for U-Mo alloys since testing was conducted in an open air environment, and since SCC in air can play a vital role in premature failure and failure mode. The strain rate selected for the current investigations $(5.83 \times 10^{-4} \text{ s}^{-1})$ is slightly lower than the maximum in ductility variation of $10^{-3} \text{ s}^{-1}$ reported by Nomine *et al.*[12] Stress corrosion cracking was found to play a significant role in decreased ductility at low strain rates, while the extent of SCC diminished as the strain rate increased because the plastic strain rate exceeds the crack velocity in stress corrosion. The effect of SCC on decreased ductility has been reported to disappear at a strain rate of $0.417 \times 10^{-3} \text{ s}^{-1}$,[12] very close the selected strain rate for the current work. Thus, SCC played no role in ductility or failure mode for the alloys prepared, investigated, and reported in this article. Oxygen behaves as an embrittling agent within the alloy, but was not considered an issue since the strain rate during tensile testing was high enough so that plastic strain within the specimen exceeded the growth of oxide film $(>5 \times 10^{-4} \text{ s}^{-1})$ and the transport of hydrogen in the material was no longer possible.[12] Carbon, although present in much lower concentrations than for the DU-12Mo or DU-7Mo alloys, will still tend to diffuse and segregate along the grain boundaries reducing the cohesive strength of the grains, and thus ultimately the culprit in the decohesive failure mode.

Finally, the DU-7Mo alloy failed mainly due to an intergranular brittle fracture, *i.e.*, decohesive rupture, but there are regions of equiaxed dimples present, more so than the other four alloys that failed in this mode (Figure 9(a)). The DU-7Mo alloy contained 100 ppm C, more than in the DU-8Mo to DU-11Mo alloys, but less than the DU-12Mo alloy. As such, the carbon that was present tended to form the second-phase particles in very discrete regions, leading to the microvoid coalescence. Similar to the DU-12Mo alloy, these second phase particles were closely distributed such that growth of the microvoids was not permitted prior to coalescence. Thus, observation of the fractograph in Figure 9(a) reveals that decohesive rupture is the main contributor to failure while dimple rupture is a secondary, accompanying failure mode.

As an additional note, there were no cleavage fracture modes observed for any of the alloys investigated in this article. This is opposite of what Nomine *et al.* reported for U-8Mo and U-10Mo homogenized alloys, where it was suggested that the {110} plane was a possible cleavage plane for bcc metals, even though the {100} plane is the most frequently observed for pure metals.[12,24] Transcrystalline cleavage is the normal brittle fracture mode of bcc metals. The absence of cleavage in the fracture surface can be attributed to the lack of homogenization prior to rolling, sample prep, and testing.

## IV.  CONCLUSIONS

Monolithic fuel alloys are poised to promote effective conversion of high power research and test reactors currently using HEU to operation with LEU, but
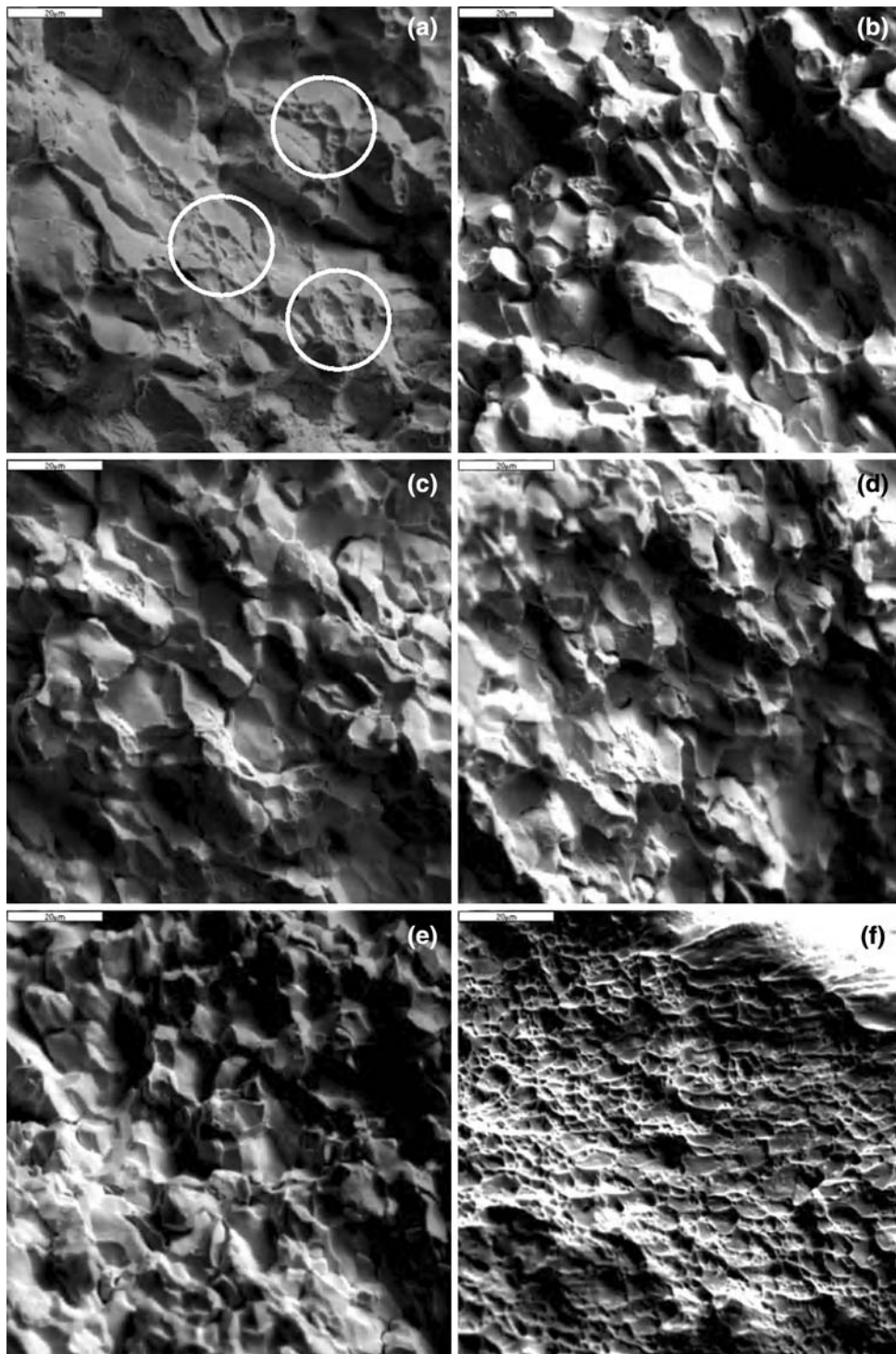
Fig. 9—SEM photomicrographs of fracture surface for (*a*) DU-7Mo alloy, (*b*) DU-8Mo alloy, (*c*) DU-9Mo alloy, (*d*) DU-10Mo alloy, (*e*) DU-11Mo alloy, and (*f*) DU-12Mo alloy. Scale bars at the top right hand corner of each photomicrograph represent 20 $\mu$m.

questions relating to the mechanical and material properties as they relate to microstructure and processing parameters and methods remain unanswered. This article takes an initial step in documenting available literature for mechanical properties of U-Mo alloys in the potential fuel alloy range, while providing additional experimental values on similar surrogate

depleted uranium-Mo monolithic fuel alloys currently being investigated. Information contained in this article might also be of interest to those seeking material property information for structural applications, especially where high-density alloys are required.

The effects on the mechanical properties of DU with Mo alloying additions ranging from 7 to 12 wt pct to

DU were investigated, and the observations of the study may be summarized as follows.

1. Microhardness of the monolithic foils increased with increasing Mo additions. Microhardness of these alloys is very sensitive to the load used during the measurement and the local alloy composition.
2. Elastic modulus, 0.2 pct offset yield strength, and ultimate tensile strength all increased with increasing Mo additions. These properties are much less dependent upon local composition, but are highly sensitive to test geometry and pretest conditions, *i.e.*, homogenization treatment. Values obtained in the current study compared reasonably well with those published in available literature, but in most cases were lower. The lower values of the current study can be attributed to the large variation in starting material conditions and sample geometry used for testing.
3. Examination of the fracture surfaces of failed samples did not reveal any consistent trends with Mo addition. A majority of the samples failed in a decohesive rupture mode, although the DU-12Mo sample failed in a dimple rupture mode, while the DU-7Mo sample failed in a mixed decohesive rupture and dimple rupture mode. Impurity concentration played a much more contributing role to failure mode than did Mo content.
4. Mechanical property information gathered will serve three main purposes: (a) effectively document available information for current and future fuel and material researcher use; (b) establish a link between fresh fuel properties and irradiated fuel observations so that the effect of irradiation can be deduced; and (c) provide a feedback loop into the foil preparation methods to optimize mechanical behaviors for additional fabrication processes and irradiation performance. However, the most obvious conclusion of this work is that further experimentation and analysis is required, given the high degree of complexity for the U-Mo system and its sensitivities to a number of conditions such as homogenization, strain rate, impurity content, specimen geometry, *etc.*

## REFERENCES

1. J.L. Snelgrove, G.L. Hofman, M.K. Meyer, C.L. Trybus, and T.C. Wiencek: *Nucl. Eng. Des.*, 1997, vol. 178, pp. 119–26.
2. A.N. Holden: *Dispersion Fuel Elements*, Gordon and Breach Science, 1968.
3. M. Ugajin, A. Itoh, M. Akabori, N. Ooka, and Y. Nakakura: *J. Nucl. Mater.*, 1998, vol. 254, pp. 78–83.
4. M.K. Meyer, G.L. Hofman, T.C. Wiencek, S.L. Hayes, and J.L. Snelgrove: *J. Nucl. Mater.*, 2001, vol. 299, pp. 175–79.
5. R.F. Hills, B.R. Butcher, and B.W. Howlett: *J. Nucl. Mater.*, 1964, vol. 11 (2), pp. 149–62.
6. J.H. Kittel, B.R.T. Frost, J.P. Mustelier, K.Q. Bagley, G.C. Crittenden, and J. Van Dievoet: *J. Nucl. Mater.*, 1993, vol. 204, pp. 1–13.
7. P.E. Repas, R.H.I. Goodenow, and R.F. Hehemann: AMRA CR63-02/1F, U.S. Army Materials Research Agency, Watertown, MA, 1963.
8. G. Beghi: EURATOM EUR 4053 e, European Atomic Energy Community (EURATOM), 1968.
9. J.A. Larrimore *et al.*: *Seminar on Intense Neutron Source*, USAEC-ENEA, Santa Fe, NM, 1966.
10. C.R. Clark, G.C. Knighton, M.K. Meyer, and G.L. Hofman: *2003 Int. Meeting on Reduced Enrichment for Research and Test Reactors*, Chicago, IL, 2003, pp. 1–10.
11. *LECO IR-412 Carbon Determinator Instruction Manual*, Leco Corporation, St. Joseph, MI, 1995.
12. A.M. Nomine, D. Bedere, and D. Miannay: *Physical Metallurgy of Uranium Alloys*, Proc. 3rd Army Materials Technical Conf., J.J. Burke, D.A. Colling, A.E. Gorum, and J. Greenspan, eds., Vail, CO, 1974, pp. 657–99.
13. R.K. McGeary: United States Atomic Energy Commission Report No. WAPD 127 Part I, Westinghouse Electric Corp.; Bettis Atomic Power Laboratory (WAPD), Pittsburgh, PA, 1951.
14. M.B. Waldron, R.C. Burnett, and S.F. Pugh: AERE-M/B-2554, Atomic Energy Research Establishment (AERE), Harwell, UK, 1958.
15. *Nouveau Traite de chimie minerale–Tome XV, quatrieme fascicule*, P. Pascal, ed., Paris, 1960, p. 377.
16. W.A. Bostrom and E.K. Halteman: *Advanced Nuclear Engineering*, *Vol. II*, J.R. Dunning and B.R. Prentice, eds., Pergamon Press, New York, NY, 1957, pp. 184–93.
17. P.C.L. Pfeil and J.D. Browne: AERE M/R 1333, Atomic Energy Research Establishment (AERE), Harwell, UK, 1954.
18. R.L. Craik, D. Birch, C. Fizzotti, and F. Saraceno: *J. Nucl. Mater.*, 1962, vol. 6 (1), pp. 13–25.
19. K.G. Hoge: *J. Basic Eng.*, 1966, pp. 509–17.
20. M.A. Meyers and K.K. Chawla: *Mechanical Metallurgy Principles and Applications*, Prentice-Hall, Inc., Englewood Cliffs, NJ, 1984.
21. C.A.W. Peterson and R.R. Vandervoort: Report No. UCRL-7771, University of California Radiation Laboratory (UCRL), Berkeley, CA, 1964.
22. M.J. Alinger, G.R. Odette, and G.E. Lucas: *J. Nucl. Mater.*, 2002, vols. 307–311, pp. 484–89.
23. *ASM Handbook*, 10th ed., vol. 12, *Fractography*, ASM INTERNATIONAL, Materials Park, OH, 1990.
24. F. Terasaki: *Metaux Corros. Ind.*, 1967, vol. 42, pp. 1–30.